Available online at www.sciencedirect.com
SCIENCE DIRECT®
Chemical Physics Letters 377 (2003) 633–641
CHEMICAL PHYSICS LETTERS
www.elsevier.com/locate/cplett

Generalized ensembles serve to improve the convergence of free energy simulations

Ryan Bitetti-Putzer [a,b], Wei Yang [b], Martin Karplus [a,b,c,*]

[a] Committee on Higher Degrees in Biophysics, Harvard University, Cambridge, MA 02138, USA
[b] Department of Chemistry and Chemical Biology, 12 Oxford St., Harvard University, Cambridge, MA 02138, USA
[c] Laboratoire de Chimie Biophysique, ISIS, Université Louis Pasteur, 67000 Strasbourg, France

Received 10 March 2003; in final form 13 June 2003

Abstract

A novel method for the calculation of the free energy difference between two states of a molecular system is presented. The method, an extension of thermodynamic integration, treats the coupling parameter λ as a variable in an extended Hamiltonian formulation and propagates it with the physical coordinates. In the resulting generalized ensemble, the crossing of barriers in the physical space is enhanced. The free energy difference is determined by integrating the reversible work required to move λ from zero (corresponding to the initial state) to one (corresponding to the final state). Examples are presented to illustrate the method.

1. Introduction

Free energy simulations of mesoscopic systems (e.g., biomolecules in aqueous solutions) are an important tool for obtaining a microscopic description of macroscopic phenomena. Specifically, the simulations, like laboratory experiments, follow a reversible path to obtain the difference in free energy between two states of the system; e.g., a molecule in the gas phase and in solution or one amino acid replaced by another in a protein. Although the original concepts employed in such simulations go back to the thermodynamic integration formalism presented in a paper published by Kirkwood [1] more than 65 years ago, it is only relatively recently that the available computational resources have made it possible to obtain meaningful results; many of these have been described in reviews [2]. The 'coming of age' of free energy simulations [3] has focussed particular attention on reducing the statistical errors in the calculations, although the systematic errors, due to inaccuracies in the potential, are also important. For converged results with small statistical errors, adequate conformational sampling of the phase space is required. This can be difficult to achieve if there are free energy barriers that must be crossed in going from the initial to the final state of the system under study. In performing the simulations, a coupling

* Corresponding author. Fax: +1-617-496-4793.
E-mail address: marci@tammy.harvard.edu (M. Karplus).

0009-2614/$ - see front matter © 2003 Elsevier B.V. All rights reserved.
doi:10.1016/S0009-2614(03)01057-1

parameter λ is generally introduced into the potential function such that $\lambda = 0$ and $\lambda = 1$ correspond to the initial and final state, respectively, and intermediate values of λ permit a reversible switching from one state to the other. The average value of the derivative of the Hamiltonian at a series of λ values are obtained by molecular dynamics (or Monte-Carlo) simulations and these averages are integrated over λ (hence the term 'thermodynamic integration') to obtain the overall free energy change. It has been suggested [4–7] that improved convergence in the free energy can be achieved by treating λ not as a parameter, but rather as a dynamical variable in addition to the coordinates and momenta of the system. That such an extension of the thermodynamic ensemble under study is possible is one of the characteristics of molecular dynamics simulations. It has been used for multiple purposes, such as the control of the system temperature and pressure [8–10], the introduction of the electronic degrees of freedom into the potential [11], and the calculation of excess chemical potentials [12]. In the present application to free energy difference simulations for two states, the potentials of the states i and j are dynamically scaled by factors λ_i^2 and λ_j^2 ($\lambda_i^2 + \lambda_j^2 = 1$), which are propagated via an extended Hamiltonian as one-dimensional particles with conjugate momenta p_{λ_i} and p_{λ_j}. The Hamiltonian is constructed (as in the parametric formulation) such that when $\lambda_i = 1$, the potential function is that of state i alone. The extended system is simulated at constant temperature, though this is not essential. Under these conditions, the extension of the phase space from the physical variables $(\mathbf{p}, \mathbf{q})$ to $(\mathbf{p}, \mathbf{p}_{\boldsymbol{\lambda}}, \mathbf{q}, \boldsymbol{\lambda})$ is expected to increase the probability of crossing the free energy barriers which exist in the physical space. This can be understood as a consequence of (1) the higher dimensionality of the phase space, which results in an increased number of paths connecting any two physical configurations $(\mathbf{p}', \mathbf{q}')$ to $(\mathbf{p}'', \mathbf{q}'')$ (analogous to the use of the fourth dimension in [12]) and (2) the biased manner in which the extended space is explored. The latter is a consequence of the fact that simulating a system with a λ-scaled potential at thermostat temperature T^{res} is thermodynamically equivalent to simulating the same system with an unscaled potential at thermostat temperature $T^{\text{eff}} = T^{\text{res}}/\lambda$ [13,14]. (For this identification to be rigorously true requires either (1) a perfect adiabatic separation between $\boldsymbol{\lambda}$ and the physical coordinates $\mathbf{q}$; or (2) a perfect (i.e., instantaneous) coupling of all momentum degrees of freedom with the thermal reservoir. In the present studies, condition (2) is satisfied approximately.) There is an effective lowering of barriers (for $\lambda < 1$) and more efficient sampling results from $T^{\text{eff}} > T^{\text{res}}$. The λ-scaling of the two states is coupled via a constraint equation, so that as the effective temperature for one state increases (i.e., due to the scaling of the potential associated with that state), that for the other state decreases. If the state with the larger λ value ($\sim$lower T^{eff}) encounters a barrier, then decreasing its λ value leads to a 'levelling' of its free energy surface, which is on average exponentially greater in magnitude than the concomitant 'sharpening' of the free energy surface of the other state. Consequently, it is expected that the overall sampling will be improved. Details concerning this behavior (including an analysis of the coupling of the $\boldsymbol{\lambda}$ and $\mathbf{q}$ degrees of freedom) will be given in a subsequent publication.

2. Theory

For concreteness, we consider a change from state A to state B which can be described parametrically in λ by a potential of the form

$$U(\mathbf{q}_A, \mathbf{q}_B, \mathbf{q}_{\text{env}}, \lambda) = (1-\lambda)U_A(\mathbf{q}_A, \mathbf{q}_{\text{env}}) + \lambda U_B(\mathbf{q}_B, \mathbf{q}_{\text{env}}) + U_{\text{env}}(\mathbf{q}_{\text{env}}), \tag{1}$$

where A and B uniquely have Cartesian coordinates $\mathbf{q}_A$ and $\mathbf{q}_B$, respectively, and share coordinates $\mathbf{q}_{\text{env}}$. Note that by construction U_i includes the self-energy of the unique part of state i, $U_{ii}(\mathbf{q}_i)$, plus its interaction with the environment, $U_{i,\text{env}}$ $(\mathbf{q}_i, \mathbf{q}_{\text{env}})$, while U_{env} is solely the self-energy of the environment. Eq. (1) could, for example, correspond to an 'alchemical' simulation [15] where one residue (unique part of state A) in a protein is mutated to another amino acid (unique part of state B), by varying λ from zero to one. In the standard thermodynamic integration (TI), the Hamiltonian for the system based on Eq. (1) has the form

$$H(\mathbf{p}_A, \mathbf{p}_B, \mathbf{p}_{env}, \mathbf{q}_A, \mathbf{q}_B, \mathbf{q}_{env}; \lambda) = \frac{1}{2}\mathbf{p}_A\tilde{\mathbf{M}}_A^{-1}\mathbf{p}_A + \frac{1}{2}\mathbf{p}_B\tilde{\mathbf{M}}_B^{-1}\mathbf{p}_B + \frac{1}{2}\mathbf{p}_{env}\tilde{\mathbf{M}}_{env}^{-1}\mathbf{p}_{env} + (1-\lambda)U_A(\mathbf{q}_A, \mathbf{q}_{env}) + \lambda U_B(\mathbf{q}_B, \mathbf{q}_{env}) + U_{env}(\mathbf{q}_{env}), \quad (2)$$

where $\tilde{\mathbf{M}}_I^{-1}$ is the diagonal mass matrix for the set of degrees of freedom I. The semicolon on the LHS of Eq. (2) distinguishes the variables from the parameter λ, which describes the transformation of the system from state A to state B. We note that only the potential function is scaled, not the corresponding momenta. The Helmholtz free energy difference between states A and B, ΔA, is

$$\Delta A = \int_0^1 \frac{\partial A}{\partial \lambda}\,\mathrm{d}\lambda = \int_0^1 \left\langle \frac{\partial H(\lambda)}{\partial \lambda} \right\rangle_{\lambda'} \mathrm{d}\lambda', \quad (3)$$

where $\langle \cdots \rangle_{\lambda'}$ is obtained as an ensemble average over the system corresponding to the potential $U(\lambda)$ at the given value of λ' in Eq. (1). In the case of linear scaling of the potential, as in Eq. (1), $\partial H/\partial\lambda = U_B - U_A$, so that

$$\Delta A = \int_0^1 \langle U_B - U_A \rangle_{\lambda'}\,\mathrm{d}\lambda'. \quad (4)$$

To introduce the extended ensemble with the $\{\lambda_i\}$ as dynamic variables, we replace the Hamiltonian in Eq. (2) by

$$H(\mathbf{p}_A, \mathbf{p}_B, \mathbf{p}_{env}, \mathbf{p}_\lambda, \mathbf{q}_A, \mathbf{q}_B, \mathbf{q}_{env}, \boldsymbol{\lambda}) = \frac{1}{2}\mathbf{p}_A\tilde{\mathbf{M}}_A^{-1}\mathbf{p}_A + \frac{1}{2}\mathbf{p}_B\tilde{\mathbf{M}}_B^{-1}\mathbf{p}_B + \frac{1}{2}\mathbf{p}_{env}\tilde{\mathbf{M}}_{env}^{-1}\mathbf{p}_{env} + \frac{p_{\lambda_A}^2}{2m_{\lambda_A}} + \frac{p_{\lambda_B}^2}{2m_{\lambda_B}} + (1-\lambda_A^2)U_A(\mathbf{q}_A, \mathbf{q}_{env}) + \lambda_B^2 U_B(\mathbf{q}_B, \mathbf{q}_{env}) + U_{env}(\mathbf{q}_{env}), \quad (5)$$

where the system is subject to the holonomic constraint

$$\sigma(\lambda_A, \lambda_B) = \lambda_A^2 + \lambda_B^2 - 1 = 0. \quad (6)$$

The use of λ_A^2 and λ_B^2 in Eq. (5) insures, in a simple way, that these variables are positive and when combined with the constraint (Eq. (6)), that each remains in the range [0,1] throughout the trajectory. From Eq. (5), it is evident that the dynamical variable λ_i has a mass m_{λ_i} associated with its kinetic energy (m_{λ_i} is an adjustable parameter), and that the force on λ_i is $\partial U/\partial\lambda_i$. Although, in general, a constraint such as that in Eq. (6) requires a metric tensor correction [16,17] when thermodynamic averages are evaluated, if $m_{\lambda_A} = m_{\lambda_B}$, as used here, no metric tensor correction is required.

After a single molecular dynamics trajectory has been run using the generalized Hamiltonian H (Eq. (5)), subject to the holonomic constraint (Eq. (6)), post-processing is performed to obtain the free energy change ΔA. We refer to this approach as the generalized ensemble thermodynamic integration (GETI) method. For simplicity, we use Eq. (6) to introduce the progress parameter λ

$$\lambda_B^2 \equiv \lambda, \quad \lambda_A^2 \equiv 1 - \lambda \quad (7)$$

and sort (bin) the data according to the $\lambda_B^2 \equiv \lambda$ value. When $\lambda = 0$, the potential function in Eq. (5) reduces to that of state A alone, and when $\lambda = 1$, it reduces to that of state B alone. The reversible work W_{rev} involved in switching the progress parameter from zero to one is equal to the configurational free energy difference between states A and B. To calculate W_{rev} requires a knowledge of the generalized force on λ, F_λ:

$$F_\lambda = \frac{\partial H}{\partial \lambda} = U_B - U_A. \quad (8)$$

The mean force when $\lambda = \lambda'$ can be calculated as a conditional average, i.e.,

$$\langle F_\lambda \rangle_{\lambda'}^{\text{cond.}} \equiv \langle F_\lambda \delta(\lambda - \lambda') \rangle, \quad (9)$$

where the definition of $\langle \cdots \rangle_{O'}^{\text{cond.}}$ holds for any value O' of the observable $O(\mathbf{q})$ and the RHS is obtained as an average over the extended ensemble. We have:

$$\Delta A = W_{rev} = \int_0^1 \langle F_\lambda \rangle_{\lambda'}^{\text{cond.}}\,\mathrm{d}\lambda' = \int_0^1 \left\langle \frac{\partial H}{\partial \lambda} \right\rangle_{\lambda'}^{\text{cond.}} \mathrm{d}\lambda' = \int_0^1 \langle U_B - U_A \rangle_{\lambda'}^{\text{cond.}}\,\mathrm{d}\lambda' \quad (10)$$

or

$$\Delta A = \int_0^1 \left\langle \frac{\partial H(\lambda)}{\partial \lambda}\delta(\lambda - \lambda') \right\rangle \mathrm{d}\lambda'. \quad (11)$$

Eqs. (3) and (11) are similar in form. In Eq. (3), however, the thermodynamic averages are with

respect to a series of ensembles described by the Hamiltonian of Eq. (2) with different values of the parameter λ, while in the latter equation (Eq. (11)), the averages are conditional averages with respect to the generalized ensemble described by the Hamiltonian of Eq. (5).

In summary, rather than restricting λ to certain values, as in standard thermodynamic integration (Eq. (3)) or a series of local intervals as used by Brooks et al. to obtain a potential of mean force [5], we perform a single simulation with λ allowed to take on any value between 0 and 1, the physically meaningful range. From this simulation, we calculate ΔA using thermodynamic integration formulated in terms of the generalized ensemble (Eq. (11)). The essential point of introducing the generalized ensemble is to make use of its greater flexibility to obtain more rapid convergence than is possible in standard (parametric) TI, as we show by the examples.

3. Methods

We consider two systems to illustrate the present methodology and, in particular, its rate of convergence. The first is a simple model system for which the free energy difference can be calculated by numerical integration and the second is a realistic problem concerning an amino acid in solution. Details of the calculational method are given at http://tammy.harvard.edu.

3.1. Butane-like model system

Two butane-like molecules, A and B, were built, each composed of four identical extended atoms with the mass of carbon. The charges of all atoms were set to zero, as were all van der Waals interactions. Bond and angle terms were set equal in the two molecules. The torsional potentials used were

$$U_{\mathrm{A}}(\phi) = 2 + \cos(\phi) + \cos(2\phi),$$
$$U_{\mathrm{B}}(\phi) = 1 + \cos(\phi - \pi). \tag{12}$$

The sole difference between the potential energy surfaces of A and B is due to the torsional potentials given in Eq. (12). The torsional energy surfaces for states A and B are shown in Fig. 1; U_{A} has a symmetric double minimum and U_{B} has a single minimum. The free energy difference $\Delta A = A_{\mathrm{B}} - A_{\mathrm{A}}$, calculated by numerical integration of the configurational partition functions for A and B, is −0.850 kcal/mol at 300 K and −0.860 kcal/mol at 150 K. These values are used to test the convergence of the free energy simulations.

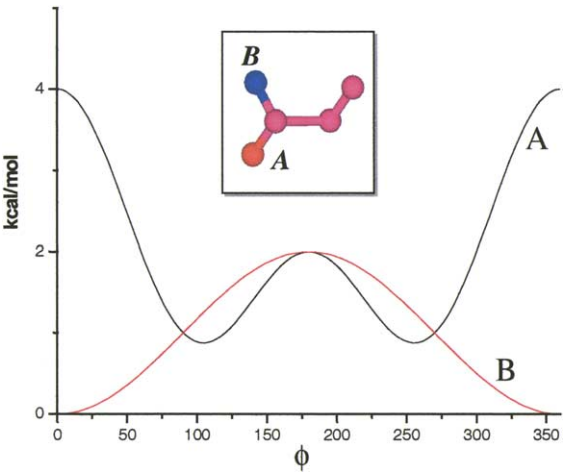

Fig. 1. Torsional energy surfaces (in kcal/mol) for states A and B in the butane-like model system. The inset shows the dual-topology (hybrid) molecule used for the simulations, i.e., only one extended carbon atom is duplicated.

3.2. Histidine solvation free energy

The second system is the amino acid of histidine in aqueous solution. Histidine consists of a five-member imidazole ring attached to the β-carbon of an amino acid (see Fig. 2, inset). The amino acid was used in the zwitterionic form. There are two protonation sites (N_δ and N_ϵ) on the imidazole ring, and both have a pK_{a} close to pH 7 (i.e., the pK_{a} for H_δ is 6.92 and that for H_ϵ is 6.53). As a result, the protonation and deprotonation of histidine in biological systems is of considerable importance. All calculations were done with the BLOCK dual-topology method using CHARMM [18]. We seek to calculate $\Delta\Delta A_{\mathrm{solv}}$, the difference in the solvation free energies of the neutral δ-protonated form and the doubly-protonated form of histidine. Evaluation of $\Delta\Delta A_{\mathrm{solv}}$ is an essential component of the theoretical estimation of pK_{a} values, which also requires knowledge of the pro-

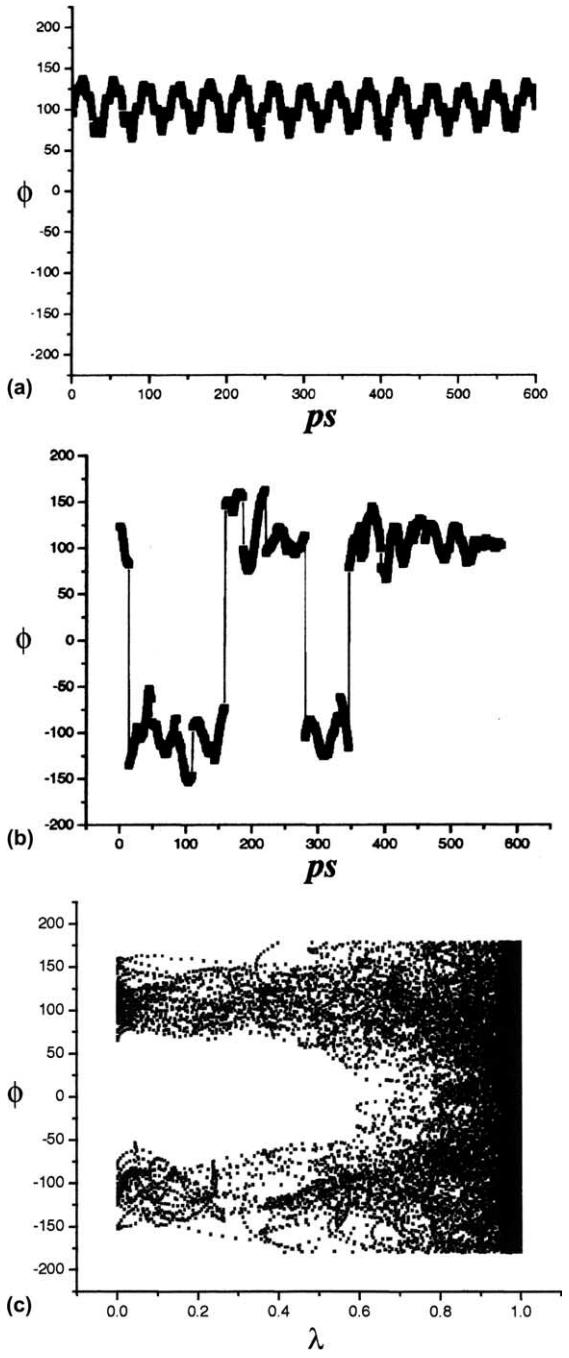

Fig. 2. Some results for the angle ϕ_A for the butane-like model system. (a) Variation in the angle ϕ_A (degrees) as a function of time (ps) in a parametric TI simulation at $\lambda = 0.01$. (b) Variation in the angle ϕ_A (degrees) as a function of time (ps) in the GETI simulation for all $\lambda < 0.05$. (c) Scatterplot of the angle ϕ_A as a function of λ in the GETI simulation.

ton free energy in water and the gas-phase quantum-mechanical free energy difference between the unionized and ionized states [19,20]. In the present methodological analysis, we focus on $\Delta\Delta A_{\text{solv}}$ which is determined by use of the thermodynamic cycle

$$\begin{array}{ccc} \text{His(gas)} & \xrightarrow{\Delta A^0_{\text{solv}}} & \text{His(aqueous)} \\ \downarrow \Delta A_1 & & \downarrow \Delta A_2 \\ \text{HisH}^+\text{(gas)} & \xrightarrow{\Delta A^+_{\text{solv}}} & \text{HisH}^+\text{(aqueous)} \end{array} \tag{13}$$

so that

$$\Delta\Delta A_{\text{solv}} = \Delta A^+_{\text{solv}} - \Delta A^0_{\text{solv}} = \Delta A_2 - \Delta A_1 \tag{14}$$

To this end, a hybrid molecule of histidine was built using a single back-bone connected to the two copies of the side chain, which differ only in their protonation states. Specifically, one copy has a proton on the δ-nitrogen, while the other has protons on both the δ- and ϵ-nitrogens. The calculation of ΔA_1, i.e., the gas-phase free energy difference, is straightforward since it involves only internal CHARMM energies. For simplicity, the zwitterionic structure is used in both the gas-phase and the solution calculations, although actually neutral terminal groups are more stable in the gas phase.

4. Results

4.1. Butane-like model system

At 300 K, the TI calculation in the generalized ensemble required 375 ps for convergence to the correct free energy difference; while the standard (parametric) TI calculation required 750 ps for convergence. At 150 K, the TI calculation in the generalized ensemble required 640 ps for convergence, at which point the standard TI calculation had not converged. For each generalized ensemble simulation, the free energy difference as determined by the probability ratio was calculated, and in neither case was it converged. For the butane-like model system, the free energy difference $\Delta A = A_B - A_A$ at 300 K, as calculated by numerical integration of the configurational partition functions for A and B, is −0.850 kcal/mol. A single simulation in the generalized ensemble allows

calculation of the free energy difference by the GETI formalism (Eqs. (5)–(11)). Using GETI, the free energy difference after 100, 200, and 375 ps is −0.861, −0.859, and −0.850 kcal/mol, respectively. Standard TI (Eqs. (2)–(4)) using a set of window simulations with cumulative times of 200, 375, and 750 ps results in values of −1.041, −0.971, and −0.850 kcal/mol, respectively.

We expect that, relative to GETI, the convergence of the standard TI calculation will become more problematic at lower temperatures, since trapping of the A state in one of the two wells becomes more likely near the $\lambda = 0$ end-point due to its relatively low effective temperature. To examine this point further, we repeated the calculations at 150 K. At this temperature, the free energy difference evaluated by numerical integration is −0.860 kcal/mol. After 200 ps, no method gives the correct value, though the GETI result is closer (−0.891 kcal/mol) versus −1.248 kcal/mol for TI. After 640 ps, the generalized ensemble calculation converged to −0.860 kcal/mol; the standard TI calculation was barely changed (−1.183 kcal/mol). The reason for this is that, in parametric window simulations near the $\lambda = 0$ end-point (i.e., where the effective temperature, $T^{\text{eff}} = T^{\text{res}}/(1-\lambda)$, of state A is slightly greater than 150 K), this state typically is trapped in a small region around one torsional minimum. This is illustrated in Fig. 2a which shows, for a window simulation at $\lambda = 0.01$, the variation in ϕ_A over 600 ps. It is clear that A is trapped throughout the trajectory around the torsional minimum at $\phi_A \approx 100°$. This is not surprising, since the free energy barrier for torsional rotation (which in this one-dimensional example is given by the potential-energy barrier) is ∼1 kcal/mol, while the average thermal energy at 150 K per degree of freedom, kT^{eff}, is ∼0.30 kcal/mol. Thus, at 150 K, barrier crossing occurs relatively infrequently (e.g., note that it does not occur even once in the 600 ps simulation at $\lambda = 0.01$ Fig. 2a). By contrast, in the GETI simulation, A does sample the full range of torsions, as a result of transient increases in the effective temperature (which reduces the effective barrier height). This can be seen clearly in Fig. 2b, which is a plot of ϕ_A values for the sequence of all trajectory points for which $\lambda < 0.05$ during the GETI simulation. The y-axis in the plot is discontinuous, because ϕ_A is plotted only for those points for which $\lambda < 0.05$. There apparently are 'thick' segments, which appear as such due to the clustering of many points. The thin lines connecting them represent (schematically) the intervals when $\lambda > 0.05$, during which $T_{\text{eff}} > T^{\text{res}}$ and transitions are more likely to occur. Fig. 2c is a scatterplot of ϕ_A for all λ values in the generalized ensemble. It is clear that when $\lambda \approx 1$ (i.e., when the effective temperature for state A is nearly infinite), no free energy barrier exists since the system uniformly samples all torsional angles. From this plot, it also is clear that below $\lambda = 0.6$, A is confined to one of the torsional conformers and thus the 'critical' effective temperature is $T^{\text{eff}} = T/(1-\lambda) \approx 375$ K. This corresponds to an average thermal energy, kT^{eff}, of ∼0.75 kcal/mol, which is adequate to cross (occasionally, as seen in Fig. 2c) a free energy barrier of ∼1 kcal/mol.

The above analysis prompts the question of why the standard TI calculation at 300 K succeeds near the $\lambda = 0$ end-point, where the effective temperature for A is less than the critical temperature for barrier crossing. Due to the twofold symmetry of the potentials associated with A and B, the resulting value of $\langle U_B - U_A \rangle$ is correct even if the system is trapped in one torsional well, i.e., it goes up to but not beyond the barrier and is converged *within this region*. Thus, the result obtained for ΔA at 150 K shows that the standard TI calculation at the $\lambda = 0$ end-point is not converged with respect to state A, even in the single well in which A is trapped. This is consistent with the distribution of the torsion angles observed in Fig. 2a, which clearly shows that only a restricted region around one torsional minimum is sampled.

4.2. Histidine solvation free energy

As mentioned in Section 3, ΔA_1 (cf. Eq. (13)) was calculated using standard TI; its value is −19.7 kcal/mol. This calculation required ∼1.7 ns for convergence. ΔA_2 (cf. Eq. (13)) calculated using standard TI is −1.2 kcal/mol and, using GETI, it is −0.87 kcal/mol. Thus, $\Delta\Delta A_{\text{solv}}$ from Eq. (14) is −20.9 kcal/mol using the standard TI method while it is −20.6 kcal/mol with the GETI method. Both results are converged, but convergence in the

GETI method was achieved in 1.2 ns, while it required about 30 ns in standard TI. In the latter, the times for individual windows ranged from ~500 ps for $\lambda = 0.5$ to ~3 ns for $\lambda = 0.995$. The GETI simulation required ~1.2 ns for convergence of $\langle U_B - U_A \rangle$. Specifically, the convergence of $\langle U_B - U_A \rangle$ for the set of bins defined by (0.1, 0.05) was assessed by reverse cumulative averaging of this quantity for each bin; the times required ranged from 0.45 to 0.70 ns for λ between 0.1 and 0.9, and increased to 1.0 to 1.2 ns at the end-points. In GETI, the convergence of the total simulation is limited by that of the slowest-converging bin.

To explore the reason for the improved convergence obtained with the GETI method, the value of the progress parameter λ (Eq. (7)) during the simulation was recorded every 10 steps. The results for the first 200 ps (i.e., 10 000 λ values) after equilibration are shown in Fig. 3. It is evident that in the generalized ensemble simulation, the system does not get 'trapped' in a given region of λ values, which can be a problem in lambda dynamics simulations. The λ value changes between zero (state A) and one (state B) on average once every 4 ps. This is illustrated in Fig. 3b, which shows the λ values over a 20 ps interval. The λ value is near one of the two end-points (i.e., in the λ region 0.00–0.05 or 0.95–1.00) for ~40% of the simulation time. Fig. 4 plots $\partial A/\partial\lambda$ versus λ for a number of bin sizing schemes (cf. Section 3). It is clear that the free energy derivative is insensitive both to the widths of the bins and to the number of bins; e.g., for the (0.1, 0.05) and (0.01, 0.005) plots, which differ most among those shown in Fig. 4, the difference in ΔA_2 is only 0.01 kcal/mol. That a more demanding stratification of the data (i.e., one in which there are many fewer data points in each bin, such as (0.01, 0.005)), yields essentially the same values indicates that the free energy derivative converges rapidly and that choice of bin size (which is an adjustable parameter of the method) is not very important. As a result, the (often serious) problem of the choice of the density of points in the standard TI method appears to be less severe in the GETI method [21].

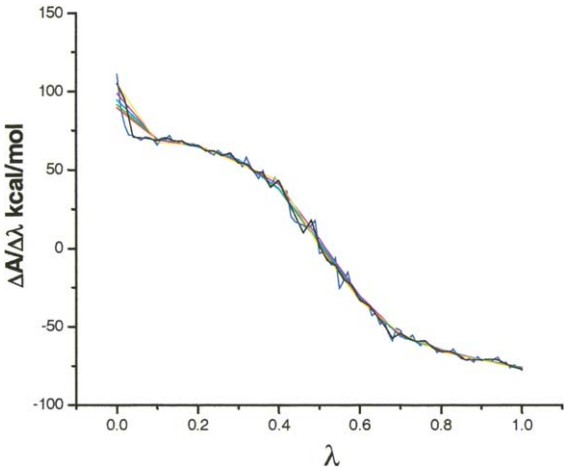

Fig. 4. The free-energy derivative, calculated from the GETI simulation, using several bin-sizing schemes: (0.1, 0.05)–red, (0.1, 0.04)–green, (0.1, 0.03)–cyan, (0.1, 0.01)–magenta, yellow, (0.02, 0.01)–black, (0.01, 0.005)–blue.

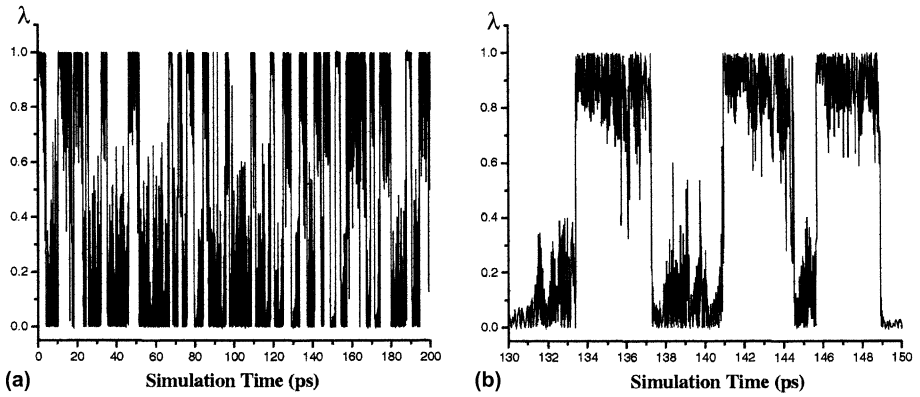

Fig. 3. Evolution of the progress parameter λ in the generalized ensemble simulation. (a) Plot over 200 ps; values every 10 fs are shown. (b) Detail of this plot over a 20 ps interval.

The single exception occurred near the $\lambda = 0$ end-point. The free energy derivative obtained using (0.1, 0.05) is well-behaved near this end-point, but smaller bin results show a 'fraying', such that the generalized ensemble curve increasingly resembles the standard curve (not shown). At $\lambda = 0$, a new particle (viz., an H^+) is introduced, which leads to well-known difficulties in obtaining converged values for the free energy derivative. Since different bin sizes can be used in analyzing a single simulation, it is possible to test whether convergence over a narrow enough sampling interval has been achieved to obtain the correct integral.

5. Discussion

We have seen that for the butane-like simple model system in the absence of solvent, the GETI method converges about a factor of two faster than the standard TI, while for the aqueous His system, the rate of convergence is increased by more than a factor of ten. There are several reasons for this behavior, some of which have been discussed in Section 1. For the purpose of comparison, the standard TI calculation can be regarded as a special case of the GETI calculation. Specifically, the parametric Hamiltonian (Eq. (2)) corresponds to a limiting case of the extended Hamiltonian (Eq. (5)), in which each lambda coordinate λ_i is adiabatically separated from the physical coordinates $\mathbf{q}_i$; i.e., each lambda 'particle' moves so slowly relative to the physical coordinates that, relative to the latter, its kinetic energy is essentially zero, and thus the physical coordinates relax in response to its 'position'. In the adiabatic limit, Eq. (5) can be replaced by an equation in which the kinetic energy of the lambda particles is absent, and the positions of the lambda particles are specified parametrically, as in Eq. (2); i.e., the coupling between the lambda coordinates and the physical coordinates is abolished. As a result, the standard TI calculation is expected to converge more slowly due to a less efficient exploration of phase space. As expected, the effect is more significant in a more complex system (e.g., His in solution versus butane in vacuum), because in general the free energy surface in a complex system is much more rugged, so that the likelihood of the system being trapped (repeatedly) in certain basins of attraction is greater. In the model butane system, we were able to show directly that the free energy barrier between the two minima was effectively reduced and more transitions occurred. We have not demonstrated the corresponding effect in the His system. However, it is well known that for simulations of polar solutes in explicit water, solvent re-organization within the first few shells (the 'solvent cage') is important in influencing ('inducing') conformational transitions in the solute [22,23]. Thus, the environment changes rapidly between configurations that stabilize the system in the A and B configurations, respectively. This is mirrored in the fact that the λ value transits between zero (corresponding to state A) and one (corresponding to state B) on average every 4 ps. Although full solvent relaxation is not achieved in such a short time period, the free energy of the solute is apparently described with high accuracy by the local solvent structure in the presence of an (unrelaxed) Hartree-like bath. This means that a much more efficient sampling of the two states is achieved with the extended Hamiltonian than in the standard TI method. Moreover, when the interaction of state i ($i = A$ or B) with a certain solvent configuration is favorable, its lambda value increases at the expense of that of the other state j (cf. Fig. 3). With $\lambda_i \approx 1$, the effective temperature of state i decreases to close to T^{res} and a nearly 'normal' distribution ρ_i for state i is achieved, i.e., one in which the parts described both by $\mathbf{q}_i$ and by $\mathbf{q}_{env}$ are sampled at (nearly) the same thermodynamic temperature, T^{res}. This type of self-optimizing competition between the two states, which is a natural consequence of lambda dynamics, has been demonstrated separately in detailed studies of ligand binding to a protein target (R. Bitetti-Putzer et al., in preparation). Since the simulation in the generalized ensemble is continued until the free energy difference has converged, the time required is determined by the slowest-converging lambda bins, which are near the end-points. Thus, in practice, the *cumulative* 'residence times' at the end-points is rate-limiting for the convergence of the simulation as a whole, and it is these which are optimally sampled by the GETI method.

In the adiabatic limit, coupling between the lambda coordinates and the physical coordinates is abolished. Sampling for each λ occurs with respect to two constant effective temperatures, viz., $T^{\mathrm{res}}/(1-\lambda)$ for state A and T^{res}/λ for state B. This results in an inherently less efficient exploration of phase space, especially for the window simulations near the end-points. In the latter, the disparity between the effective temperatures of the two states is large; e.g., state B with $\lambda \sim 1$ is at a (much) lower effective temperature and thus is susceptible to trapping, as was clearly demonstrated in the model 'butane' system.

A related advantage of the generalized ensemble method is that it inherently optimizes the time spent at each lambda value, i.e., in accord with a Boltzmann distribution for the extended ensemble, while in the standard method the user must determine the time for each window simulation. In this sense, the generalized ensemble calculation is akin to a Monte-Carlo integration strategy for multi-dimensional integrals, in which importance sampling is built into the structure of the transition matrix.

It will be of interest to determine the efficiency of GETI in other applications, as well as when different free energy simulation methods (e.g., single topology) are used.

Acknowledgements

We thank Dr. R. Yelle for assistance with the local computing environment at Harvard, where the calculations were done. The research was supported in part by a grant from the National Institutes of Health.

References

[1] J.G. Kirkwood, J. Chem. Phys. 3 (1935) 300.
[2] T.P. Straatsma, J.A. McCammon, Ann. Rev. Phys. Chem. 43 (1992) 407.
[3] T. Simonson, G. Archontis, M. Karplus, Acc. Chem. Res. 35 (2002) 430.
[4] B. Tidor, J. Phys. Chem. 97 (1993) 1069.
[5] X. Kong, C.L. Brooks III, J. Chem. Phys. 105 (1996) 2414.
[6] Z. Guo, C.L. Brooks III, J. Am. Chem. Soc. 120 (1998) 1920.
[7] Z. Guo, C.L. Brooks III, J. Phys. Chem. B 102 (1998) 2032.
[8] S. Nosé, Mol. Phys. 52 (1984) 255.
[9] S. Nosé, Mol. Phys. 57 (1986) 187.
[10] W.G. Hoover, Phys. Rev. A 31 (1985) 1695.
[11] R. Car, M. Parrinello, Phys. Rev. Lett. 55 (1985) 2471.
[12] R. Pomès, E. Eisenmesser, C.B. Post, B. Roux, J. Chem. Phys. 111 (1999) 3387.
[13] A.E. Mark, W.F. van Gunsteren, H.J.C. Berendsen, J. Chem. Phys. 94 (1991) 3808.
[14] M. de Koning, A. Antonelli, S. Yip, Phys. Rev. Lett. 83 (1999) 3973.
[15] J. Gao, K. Kuczera, B. Tidor, M. Karplus, Science 244 (1989) 1069.
[16] M. Fixman, Proc. Natl. Acad. Sci. USA 71 (1974) 3050.
[17] M. Sprik, G. Ciccotti, J. Chem. Phys. 109 (1998) 7737.
[18] B.R. Brooks, R.E. Bruccoleri, B.D. Olafson, D.J. States, S. Swaminathan, M. Karplus, J. Comp. Chem. 4 (1983) 187.
[19] P. Lyne, M. Karplus, J. Am. Chem. Soc. 122 (2000) 166.
[20] C. Lim, D. Bashford, M. Karplus, J. Phys. Chem. 95 (1991) 5610.
[21] H. Resat, M. Mezei, J. Chem. Phys. 99 (1993) 6052.
[22] J.P. Bergsma, B.J. Gertner, K.R. Wilson, J.T. Hynes, J. Chem. Phys. 86 (1986) 1356.
[23] J. Chandresekhar, W.L. Jorgensen, J. Am. Chem. Soc. 107 (1985) 2974.